Available online at www.sciencedirect.com
SCIENCE DIRECT®
Journal of Solid State Chemistry 178 (2005) 93–99
JOURNAL OF SOLID STATE CHEMISTRY
www.elsevier.com/locate/jssc

EXAFS and Raman studies of mechanical alloyed $Ni_{25}Se_{75}$ mixture under high-pressure conditions

C.E.M. Campos[a,*], J.C. de Lima[a], T.A. Grandi[a], K.D. Machado[a], J.P. Itié[b], A. Polian[b]

[a]*Departamento de Física, Universidade Federal de Santa Catarina, Campus Universitario-Trindade, C.P. 476, 88 040-900 Florianópolis, SC, Brazil*
[b]*Laboratoire de Physique des Milieux Condensés, Unversité Pierre et Marie Curie, Campus Boucicaut, 75015 Paris, France*

Received 25 August 2004; received in revised form 27 September 2004; accepted 3 October 2004

Abstract

Extended X-ray Absorption Fine Structure and Raman studies were performed to follow the structural and vibrational behavior of a mechanical alloyed $Ni_{25}Se_{75}$ mixture, containing nanocrystalline pyrite $NiSe_2$ phase, when exposed to high-pressure conditions. An increase in the local structural order of the nanocrystalline phase with pressure increasing was observed by means of Debye–Waller factor analysis. The relative Ni nearest-neighbors distances were determined as a function of pressure, which were used to determine the inverse linear compressibility of the nanocrystalline pyrite $NiSe_2$ alloy as well as its derivate by means of Murnaghan's equation. The Raman results showed tentative $NiSe_2$ phonons dispersion with pressure that becomes a difficult task since the existence/photo-induced nucleation of an important amount of nanocrystalline Se, detected due to the observation of its pressure-induced phase transitions.

Keywords: X-ray absorption spectroscopy (EXAFS); High-pressure effects in solids; Mechanical alloying; Nanocrystalline materials

1. Introduction

Transition metal (*TM*) dichalcogenides have been widely studied due to their large occurrence in geological environments [1] and also because its very interesting applications in high-energy density batteries, photo-eletrolysis, solar energy materials, precursors of super-conducting syntheses, luminescence materials, and chalcogenide glasses [2]. These compounds can be found with the pyrite- and marcasite-type structures, but recent studies in a close-related compound (diantimonide, *TM*-Sb_2) [3] have shown the existence of an intermediary arsenopyrite-type structure, which is considered a high-pressure polymorph of the marcasite one. The pyrite structure is based on that of NaCl, with anions replaced by X_2 dimers (X = S, Se, Te and Sb) whose axes are oriented along the four {111} cube directions. Each *TM* atom is surrounded by six X ones in a slightly distorted octahedron, and each X atom is coordinated by three *TM* atoms and its dimer pair. The marcasite is considered a metastable polymorph of *TM*-X_2 compounds and assumes an orthorhombic structure. The two polymorph structures show basically the same local environment of pyrite, but they present stronger distortions in the octahedron and tetrahedron configurations of their *TM* and X atoms, respectively.

Recently, we have showed that several *TM*-Se_2 alloys can be produced in the nanocrystalline form starting from $TM_{25}Se_{75}$ powder mixtures and using a simple mechano-synthesis process [4–11]. The mechano-synthesis process [12], also known as mechanical alloying (MA), is based in a solid state reaction where the powder particles are subjected to severe mechanical deformation during collisions with balls and vial, which are shacked by a mill; consequently the particles are repeated deformed, fractured and cold-welded. As a result of this solid-state reaction amorphous and/or

*Corresponding author. Fax: +55 48 331 90 68.
E-mail address: pcemc@fisica.ufsc.br (C.E.M. Campos).

0022-4596/$ - see front matter © 2004 Elsevier Inc. All rights reserved.
doi:10.1016/j.jssc.2004.10.006

nanocrystalline alloys can be obtained. The remarkable characteristics of the alloys produced are the highly disordered interfacial region surrounding the nanoparticles, the high defect concentrations and high-strained structures [13]. It is interesting to note that depending of the *TM* atom used the structural evolution of the mixtures with milling time assumed different paths. For the $Fe_{25}Se_{75}$ mixture the $FeSe_2$ marcasite-type structure was observed in the first 40 h of milling, passing by a stage of coexistence of marcasite- and monoselenides (with NiAs-type structures) alloys, and after 72 h of milling the NiAs-type structures (FeSe and Fe_7Se_8) became predominant. For the $Co_{25}Se_{75}$ mixture the $CoSe_2$ alloy showed the coexistence of marcasite- and pyrite-type structures up to 38 h of milling, a single pyrite $CoSe_2$ for 52 h of milling and also was transformed to NiAs-type monoselenide (CoSe) phase for longer milling times (80 h). In the $Ni_{25}Se_{75}$ system only the pyrite $NiSe_2$ alloy was observed for milling times as longer as 92 h, indicating a great structural stability of this phase. In all systems an interesting effect of rearrangement of the Se balance portion as amorphous Se (a-Se) and/or linked to contaminants was observed, but for longer milling times its structural form and localization could not be well determined and some possibilities have been proposed to explain this phenomenon. The Se balance atoms can be dispersed in the interfacial regions of the nanocrystals as non-reacted Se and/or can be linked with the contaminants providing from the milling tools or from the milling atmosphere.

One of the goals of this paper was to test the structural stability of the nanocrystalline pyrite $NiSe_2$ alloy following the behavior of the local environment of the Ni atoms up to 19 GPa by means of high-pressure XAS experiments. The study of phase transformations following the modifications in short-range order, as given by analyzing a special region of XAS spectra—EXAFS, has several advantages over the studies of long-range order, obtained by diffraction experiments. The main advantage is that it directly provides the coordination numbers around a selected absorbing atom. A visual evaluation of the XAS spectra in the XANES region can furnish strong evidences of the electronic character of the absorber atom bonding. Furthermore, considering the evolution of the local disorder parameter (relative Debye–Waller) as a function of pressure is possible to determine more accurately the exact pressure for which a phase transition starts.

Plotting the relative Ni nearest-neighbours distances as a function of pressure and fitting it using the Murnaghan's equation, the inverse linear compressibility of the nanocrystalline pyrite $NiSe_2$ alloy and its derivate were determined.

In order to complement the structural studies, the Raman studies were performed to follow the high-pressure vibrational profile of the sample. Considering that the stabilization of the $NiSe_2$ phase from $Ni_{25}Se_{75}$ powder mixture is attributed to the existence of non-reacted Se in a strange form and/or localization that could not be determined at ambient conditions, and that Raman measurements are very sensitive to Se phonons, these studies were very useful to better explain the atomic diffusion caused by the mechano-syntheses process.

2. Experimental details

The $Ni_{25}Se_{75}$ sample milled for 92 h was submitted to high hydrostatic pressures generated by axial forces acting between two small diamonds of a Diamond Anvil Cell (DAC). The high-pressure X-ray Absorption Spectroscopy (XAS) experiments are performed in transmission mode and consequently the X-ray beam must pass by the diamonds. Then, several problems arrive. The ordinary XAS setup using the classic two-crystal monochromator and ionization cameras is strongly dependent of mechanical movements which difficult enormously the beam focalization. The diamond Bragg reflections must be attenuated or dislocated from the spectral range of interesting by changing the relative position of the DAC with respect with the X-ray beam. As each classical XAS spectrum demands at about 5 min and many DAC positions are, in general, tested, it will be an energetically and time expensive task. The utilization of a Dispersive XAS setup to collimate the polychromatic beam in a few tens of microns without any mechanical movement coupled with a position-photosensible detector is indispensable to realize pressure-induced structural studies. In this setup the acquisition time is minimal (tens of 10^{-3} s) offering high stability and reproducibility in the measurements that allows to cleaning completely a large energy domain from glitches due to the diamond Bragg reflections in a short period of time.

EXAFS experiments were performed in Ni *K*-edge (8333 eV) at D11 station of DCI in Laboratoire pour l'Utilisation du Rayonnement Electromagnétique (LURE), Orsay, France.

The posterior data treatments were done by using the CDXAS-26 [14] software package.

Raman scattering measurements were performed at ambient temperature in a XY Dilor monochromator coupled to an optical focal lens ($20\times$) and CCD counting system. The 514.5 nm line of an argon ion laser was used as exciting light always in backscattering geometry and using an output power below the 5 mW to avoid the overheating of the sample.

The pressure determination during the XAS (Raman) measurements was performed through the pressure-dependent fluorescence of a ruby chip and silicone oil (argon) was used as pressure transmitting medium.

3. Results and discussion

3.1. XAS measurements

Fig. 1 shows the XAS spectra of the $Ni_{25}Se_{75}$ sample milled for 92 h at ambient pressure and four representative pressures up to 19.1 GPa. From this figure one can see that a very good spectral range was obtained, at about 800 eV after Ni K-edge. It is also clear that no important structural changes occurred.

Fig. 2 shows the XANES region of the XAS spectra as a function of pressure. This region of the XAS contains information concerning photo-electron multiscattering effects, which gives access to medium-range order (~15 Å) of the atomic systems. Then, it is clear from Fig. 2 that the $NiSe_2$ alloy produced by MA has a very good structural stability with respect to pressures as high as 19 GPa even in the medium range distances. The edge values observed for the milled sample are in quite good agreement to that of Ni metal, indicating that there are no electronic features at energy levels smaller than those of metallic form.

Fig. 3 shows the EXAFS region of the XAS spectra as a function of pressure. It was observed both phase-shift and amplitude magnification with pressure increasing. Once more, the resemblance between the spectra showed that no phase transition occurred in the pressure range tested.

The structural effects caused by the pressure increasing become more evident after the EXAFS data treatments where the radial distribution functions were obtained by means of Fourier transforming (FT) operations (Fig. 4). The shortening of Ni nearest-neighbors average distance and the intensity increasing of the signal amplitude can be easily observed.

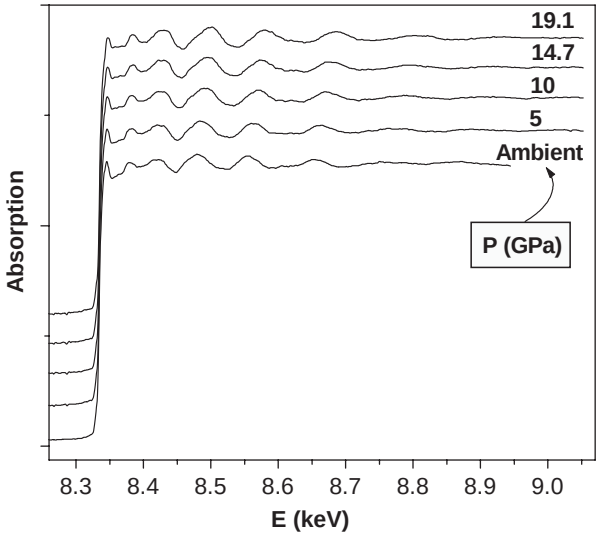

Fig. 1. XAS spectra of the $Ni_{25}Se_{75}$ sample milled for 92 h as a function of pressure.

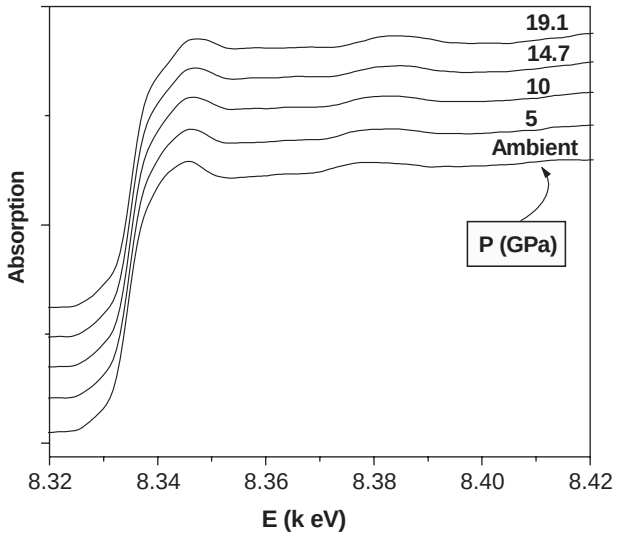

Fig. 2. XANES region of the XAS spectra of the $Ni_{25}Se_{75}$ sample milled for 92 h as a function of pressure.

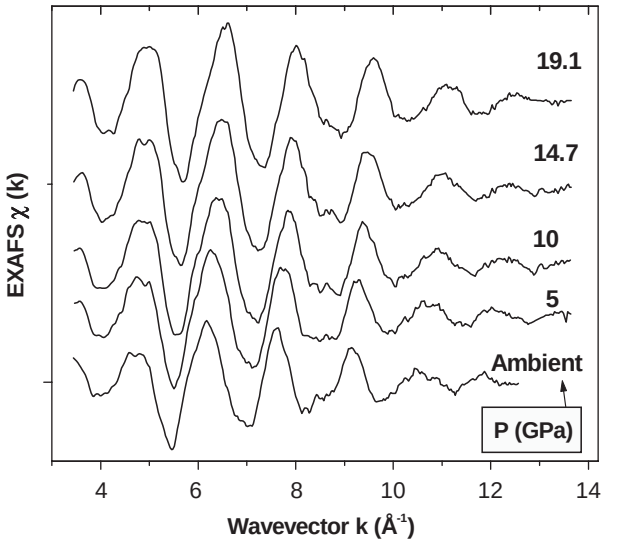

Fig. 3. EXAFS region of the XAS spectra of the $Ni_{25}Se_{75}$ sample milled for 92 h as a function of pressure.

Fig. 5 shows the filtered EXAFS signals, $\chi(k)$, as a function of pressure. They were obtained by inverse FT operations performed in a selected (FT mean peak) region, which represents the first coordination sphere. Using the phase and amplitude extracted from the EXAFS signal at ambient conditions and considering the short-range crystallographic information for the pyrite $NiSe_2$ phase [15,16] (coordination number $N = 6$ and average distance $d = 2.48$ Å), simulated EXAFS signals were proposed for experimental signals collected at higher pressures (see symbols in Fig. 5). The simulations were performed fixing the N and the electronic parameters. From these simulations the

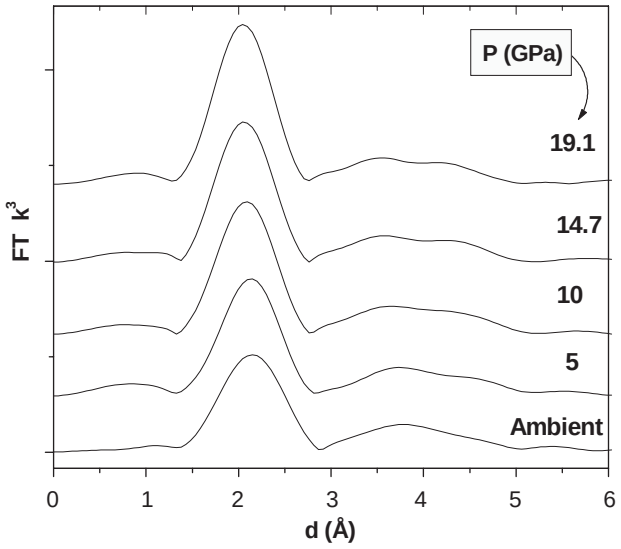

Fig. 4. Fourier transforming signals of the $Ni_{25}Se_{75}$ sample milled for 92 h as a function of pressure.

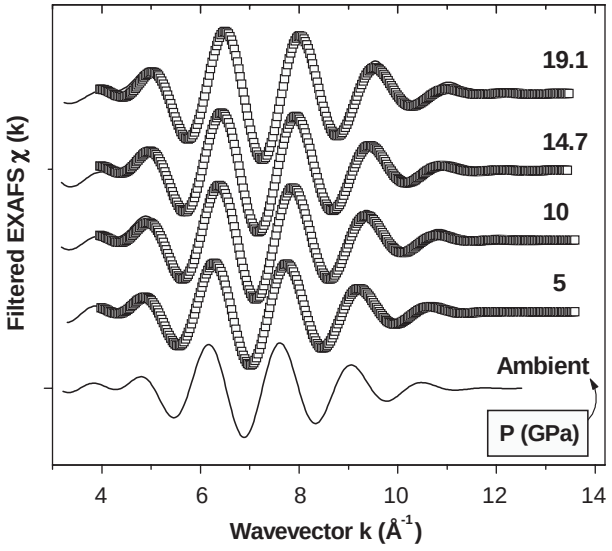

Fig. 5. Filtered EXAFS signals of the $Ni_{25}Se_{75}$ sample milled for 92 h as a function of pressure. Symbols represent the simulated EXAFS signal.

variation of Ni nearest-neighbours average distance (d) and the relative Debye–Waller ($\Delta\sigma^2$) parameters were determined as a function of the pressure.

Fig. 6a shows the relative Debye–Waller ($\Delta\sigma^2$) parameter as a function of pressure. The reduction of the $\Delta\sigma^2$ parameter with pressure indicates a local environment order increasing around the Ni atom. Then, this fact discards the possible phase transition from the pyrite to marcasite and/or to marcasite polymorph, which are more disordered than the pyrite one.

Fig. 6b shows the relative variation of the Ni nearest-neighbors distance (d/d_0) of nanocrystalline $NiSe_2$ alloy

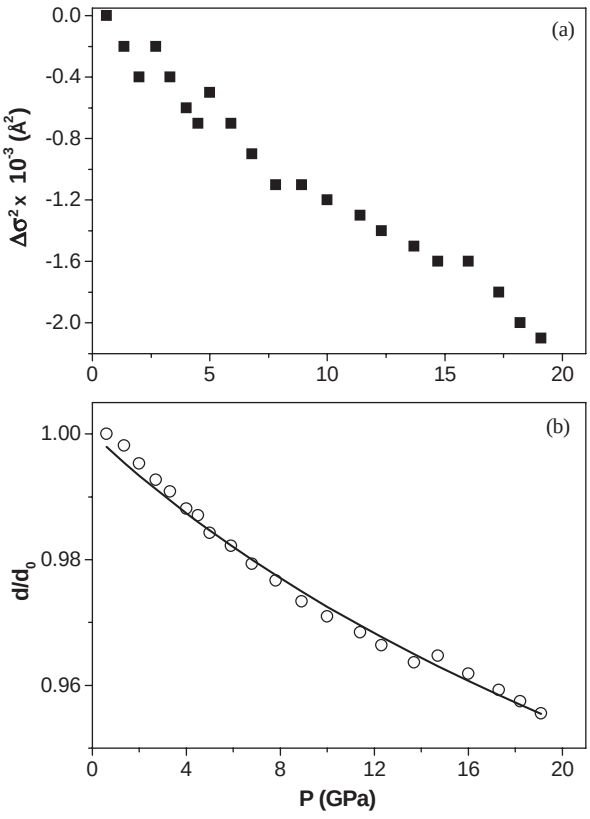

Fig. 6. Relative Debye–Waler factor (a) and Ni nearest-neighbours distance (b) as a function of the pressure. Solid line represents the best fitting reached by using Murnaghan's equation.

as a function of pressure. A reduction of about 5.5% in the nearest-neighbours distance was observed when the pressure reached 19.1 GPa. Using the Murnaghan's equation the inverse linear compressibility (B_{L0}) and its derivate in relation to pressure (B'_L) were determined:

$$d(P) = d_0\left(1 + \frac{B'_L P}{B_{L0}}\right)^{-1/3B'_L}.$$

The value obtained was $B_{L0} = 95$ GPa ($B'_L = 5.3$) for nanocrystalline pyrite $NiSe_2$. The B_{L0} value is smaller than that obtained for the marcasite $FeSe_2$ alloy also produced by mechano-synthesis where $B_{L0} = 196.4$ GPa (fixing $B'_L = 5.5$). It is interesting to note that the bulk-modulus of Ni is about 10% greater than that of Fe. However, the B_{L0} parameters observed for the selenide alloys produced by milling, with a simple substitution of the metal cations, does not follow the same tendency of the pure metals. One good explanation for this fact, based on iron disulfides alloys, is that pyrite structure is more compressible than the marcasite one.

As in the pyrite-type structures there is a great structural symmetry, the linear effects can be projected in all three directions and the B_{L0} value can be compared to the bulk-modulus of other dichalcogenides.

The disulfides also show greater B_0 values for both marcasite (163.0 GPa) and pyrite (159.0 GPa) FeS_2 structures, but no values were done to its derivate B' [17]. On the other hand, in Ref. [18] $B_0 = 215$ GPa is reported for the pyrite FeS_2 with quite equal pressure derivates ($B' = 5.5$). The discrepancies and poor information about pyrite bulk modulus in the literature did not allow any conclusion about the influence of particle size in the compressibility parameter.

3.2. Raman measurements

The pyrite structure *Pa3* (T_h^6) has five active Raman modes. Due to its localization in the structural center of inversion the Ni atoms have no important contribution in the vibrational pattern, which represents only the movements of the chalcogenide ions. This fact indicates that the Raman spectrum is very sensitive to the chemical environment and structural order of these ions. The active Raman modes can be classified according with the symmetries of atoms movements (vibrations). In the pyrite A_g and T_g modes correspond, respectively, to in-phase and out-phase stretching vibrations of the ions. There are other two T_g modes, plus an E_g mode associated with the ions librations.

In the specific case of pyrite nickel diselenide ($NiSe_2$) a recent report [19] have been the pioneer to register its Raman spectrum in thin films produced by selenation of Ni thin films and also to study the effects caused by the replacement of Se ions by S ones. The authors reported grain sizes from 500 to 1000 Å and some textures in the films surface. They also showed that the in-phase stretching vibrations (214 cm^{-1}) are the most important contribution to the $NiSe_2$ Raman spectrum, followed by the out-phase stretching (243.3 cm^{-1}) and libration (151.9 cm^{-1}) T_g modes and, the E_g libration mode (170.2 cm^{-1}) is the weaker vibrational contribution. However, curiously the authors omitted a very pronounced peak, located at about 250 cm^{-1}, which appears as a shoulder of out-phase stretching mode.

On the other hand, it has been reported in a previous paper [6] that nanocrystalline $NiSe_2$ can be produced by MA of a $Ni_{25}Se_{75}$ mixture and its Raman spectrum have presented the same stretching and libration modes, including the 250 cm^{-1} line. The $NiSe_2$ modes were observed even for 3 h of milling and remained as the only features of the spectra of the samples milled up to 92 h, which is in good agreement with the X-ray diffraction results. Unfortunately, the previous Raman analysis could not clarify the questions about the structure and localization of Se-excess since the Se modes are in the same spectral region of the $NiSe_2$ ones.

Bulk Se is known to have five pressure-induced phase transitions. The transformation sequence with increasing pressure is hexagonal → monoclinic(I) → monoclinic(II) → orthorhombic → rhombohedral and cubic at 14, 23, 28, 60 and 140 GPa, respectively [20–22]. In one of the papers [21], reporting energy dispersive and Raman experiments, the pressure induced structural transitions of Se in nanocrystalline form (up to 30 GPa) showed a more complex phase transition behavior with lower transitions pressures and lower symmetry of high-pressure phases as compared to bulk Se. The authors attributed these effects to the structural instability of nanocrystalline phases. Then, following this pressure-induced phase transition scene, the high pressure Raman measurements of the MA $Ni_{25}Se_{75}$ sample can proof the (in)existence of non-reacted Se in the sample, as well as, determine its structure and dimensional scale (particles size).

Fig. 7 shows the Raman spectra of $Ni_{25}Se_{75}$ milled for 92 h as a function of pressure. The plasma line of the laser is indicated as PL in this figure. The first spectrum, at the bottom of this figure, was collected out of DAC and, curiously, it was not well reproduced when the sample was introduced in the cell without pressure transmission medium. Fortunately, after the Argon charging (see spectrum at 0.9 GPa) the Raman profiles of the sample were recovered. The spectrum at 0.9 GPa

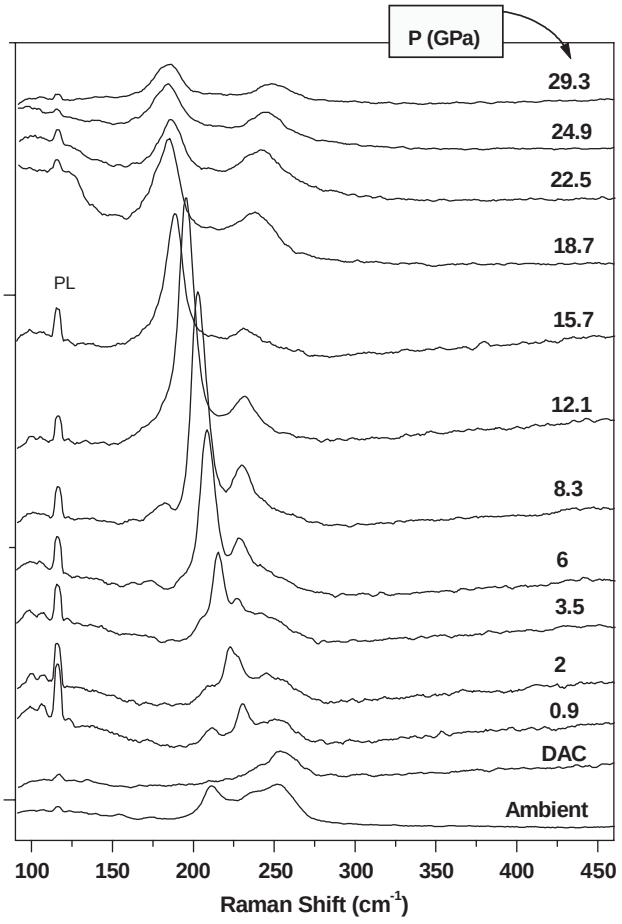

Fig. 7. Raman spectra of the $Ni_{25}Se_{75}$ sample milled for 92 h as a function of pressure.

shows the A_g and T_g modes corresponding, respectively, to in-phase and out-phase stretching vibrations of the ions; but the other two low-frequency modes, associated with the ions librations, were not well defined due to their small intensity. A slight intensity increasing of one line (located at about 230 cm^{-1}) between the two stretching modes was observed. Although this line seems to be present in the spectrum at ambient conditions it will be called "new line" in the following.

Comparing the frequency of the new line with that of $A1$ mode produced by helical chain-expansion type lattice vibrations of Se, one can conclude that this peak is produced by Se-excess in the $Ni_{25}Se_{75}$ sample milled for 92 h. Furthermore, the behavior of this line with pressure increasing is identical to that of nanocrystalline Se (nc-Se) phase, as will be discussed below. Considering that neither crystalline nor amorphous Se were observed by DSC and XRD measurements of this sample [6], the most probable explanation is that there was an important amount of Se nanocrystals well dispersed in the interfacial region of the $NiSe_2$ crystallites and/or during the Raman experiments the laser power could be responsible by photo-induced nc-Se nucleation/agglomeration from Se atoms dispersed in the interfacial region. These interpretations are in agreement with the well-known characteristic of nanomaterials determined by total structural factors (TSF) analyses of as-milled and pos-annealed samples [23]. The TSF analyses have shown that in the as-milled mixture the number of atoms in both components (interfacial and nanocrystallites) is similar.

With pressure increasing the Raman lines corresponding to the $NiSe_2$ modes became larger than before forming a very large band between 190 and 280 cm^{-1}. In addition, the nc-Se modes became so intense that attenuated all other lines of the high-pressure spectra, which difficult the correct determination of the pressure induced dispersion curve for the $NiSe_2$ phonons. The Raman lines broadening with pressure, as observed for the $NiSe_2$ modes, is a common effect attributed mainly to anharmonic processes that reveal the influence of the phonon dispersion on decay process due to changes in phonon frequencies throughout the Brillouin zone [24]. Then, it is important to note that the linebroadening of $NiSe_2$ modes is not contradictory with the EXAFS results of $NiSe_2$, which showed a crystallinity improvement with pressure increasing. In order to visualize all the changes induced by pressure in the Raman spectra, a fitting procedure was performed using Lorentizian functions and its result is shown in Fig. 8. Fig. 9 shows more detailed results obtained for the nc-Se modes.

With pressure increasing the $A1$ mode shifts to lower frequency, indicating a pressure-induced strengthening of the interchain bonds and a weakening of the intrachain ones. This behavior is responsible for the huge intensity increasing of the $A1$ mode with pressure,

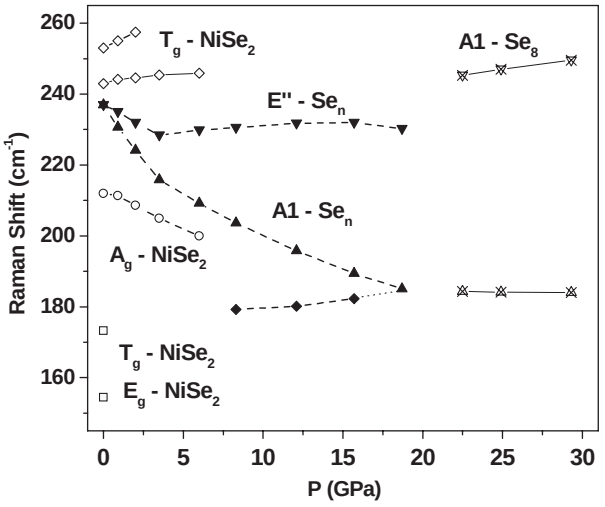

Fig. 8. Phonons frequency of the $NiSe_2$ (empty symbols) and nc-Se (full symbols) as a function of pressure.

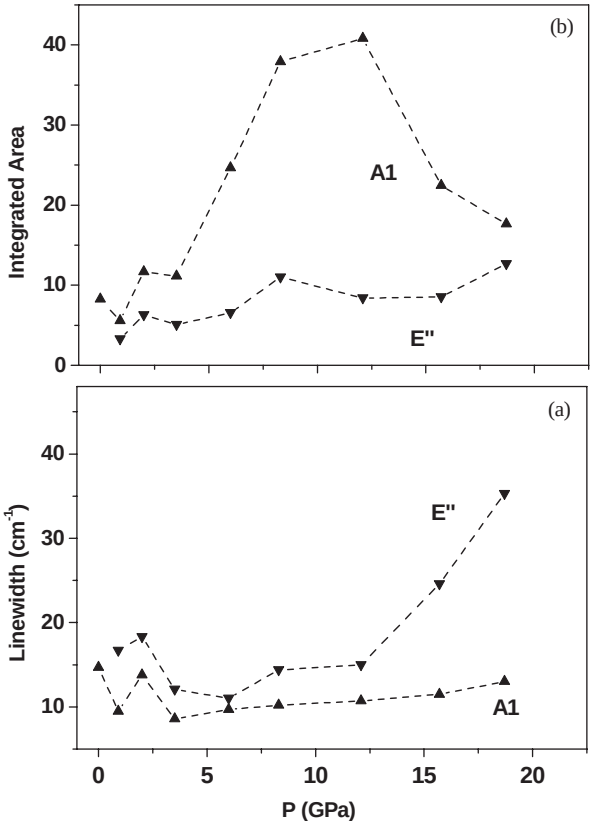

Fig. 9. Raman linewidth (a) and integrated area (b) of the nc-Se modes as a function of pressure.

in agreement with previous reports for bulk and nanocrystalline Se [20,21]. The strange change of the $A1$ mode at about 15.7 GPa suggests a phase transition, which was identified as an intermediate phase Se(III) observed only in the nanocrystalline form [21]. The $A1$ mode continues the softening trend, and disappears at

22.5 GPa, indicating a structural distortion of the helical-chain. This interpretation was done based in energy dispersive X-ray diffraction (EDXD) and Raman studies of nc-Se [21], which showed that for pressures higher than 17.5 GPa the chain-like microstructure completely disjoints.

The E' mode is attributed to the rotational motion about axes perpendicular to the helical axis, whereas the E'' mode is due to asymmetric breathing motions. The peaks of the E'' and $A1$ modes overlap at ambient pressures, and then split with pressure increasing. A phase transition is evidenced at 6 GPa where the E'' mode has a minimum as function of pressure and a weak peak appears at about 170 cm^{-1} (Fig. 7). Above 18.7 GPa, the weak broad band (where E'' peak was located) moves from 240 to 250 cm^{-1}. Considering that a structural change from the helical-chain microstructure to a denser-packed layer type one has been observed at about the same pressure [21], the band at 250 cm^{-1} can be associated to the $A1$ mode of the Se_8 rings type microstructure. Moreover, the appearing of a band at 120 cm^{-1} and weak peaks (forming a low-frequency shoulder of the main line located between 180 and 190 cm^{-1}) in the spectrum at 18.7 GPa suggests a intermediate phase transition to a lower symmetry nc-Se(IV) [21,22]. Fig. 9 shows the Raman linewidth (full-width at half-maximum) and integrated area of the nc-Se modes as a function of pressure. This figure corroborates the pressure induced phase transition scene traced for the nc-Se phase by means of EDXD measurements [21].

The Raman results reinforce the previous speculation about the Se-balance, which propose its dispersion in the interfacial regions of $NiSe_2$ nanocrystals, and showed that the dispersed Se particles are in the nanocrystalline form under high-pressure conditions. However, the situation at ambient conditions remains undefined. Both amorphous and crystalline Se is mainly composed by Se chains, i.e., they have practically the same Raman spectra. In addition, photo- and pressure-induced crystallisation of Se has been already reported, which impossibilities to precisely determine the state of Se-balance at ambient conditions.

4. Conclusions

The structural and vibrational studies of the $Ni_{25}Se_{75}$ sample milled 92 h as submitted to high pressure conditions were done and the main conclusions were:

No phase transition was observed up to 19 GPa.

The nanocrystalline pyrite $NiSe_2$ is more compressible than the marcasite $FeSe_2$ also made by MA.

The high-pressure Raman experiments showed that Se-balance is found in nanocrystalline form, which, at ambient conditions, may be well dispersed in the interfacial region and/or might have been formed by photo- and/or pressure-induced nucleation/agglomeration of Se atoms.

Illustrative pictures of the pressure induced phonon dispersion curves were traced for both $NiSe_2$ and Se nanocrystalline phases.

Acknowledgment

We thank the Brazilian agency CAPES for financial support.

References

[1] H.M. Sithole, P.E. Ngoepe, K. Wrigth, Phys. Chem. Miner. 30 (2003) 615.
[2] P. Balaz, Z. Bastl, T. Havlik, I. Toth, Mater. Sci. Forum 235–238 (1997) 217.
[3] H. Takizawa, K. Uheda, T. Endo, Intermetallics 8 (2000) 1399.
[4] C.E.M. Campos, J.C. de Lima, T.A. Grandi, K.D. Machado, P.S. Pizani, Solid State Commun. 123 (2002) 179.
[5] C.E.M. Campos, J.C. de Lima, T.A. Grandi, K.D. Machado, P.S. Pizani, Physica B 324 (2002) 409.
[6] C.E.M. Campos, J.C. de Lima, T.A. Grandi, K.D. Machado, P.S. Pizani, R. Hinrichs, Solid State Commun. 128 (2003) 229.
[7] C.E.M. Campos, V. Drago, J.C. de Lima, K.D. Machado, T.A. Grandi, P.S. Pizani, J. Magn. Magn. Mater. 270 (2004) 89.
[8] C.E.M. Campos, J.C. de Lima, T.A. Grandi, K.D. Machado, P.S. Pizani, Solid State Commun. 131 (2004) 265.
[9] C.E.M. Campos, J.C. de Lima, T.A. Grandi, K.D. Machado, P.S. Pizani, R. Hinrichs, Solid State Ion. 168 (2004) 205.
[10] K.D. Machado, J.C. de Lima, T.A. Grandi, C.E.M. Campos, C.E. Maurmann, A.A.M. Gasperini, A.A.M. Souza, A.F. Pimenta, Acta Crystall. B 60 (2004) 282.
[11] J.C. de Lima, V.H.F. dos Santos, T.A. Grandi, NanoStruct. Mater. 11 (1999) 51.
[12] C. Suryanarayana, Prog. Mater. Sci. 46 (2001) 1.
[13] H. Gleiter, Prog. Mater. Sci. 33 (1989) 223.
[14] A. San-Miguel, Physica B 208&209 (1995) 177.
[15] ICSD—Inorganic Crystal Structure Database, Gmchin-Institute fur Anorganishe Chemie and Fachinformationszentrum FIZ, 1995.
[16] Atomic Softek, 70 Longwood Road North, Hamilton, Ont., Canada L8S 3V4.
[17] H.M. Sithole, P.E. Ngoepe, K. Wright, Phys. Chem. Miner. 30 (2003) 615.
[18] H. Fjellvag, W.A. Grosshans, W. Hönle, A. Kjekshus, J. Magn. Magn. Mater. 145 (1995) 118.
[19] C. de las Heras, F. Agulló-Rueda, J. Phys.: Condens. Matter 12 (2000) 5317.
[20] A.K. Bandyopadhyay, L.C. Ming, Phys. Rev. B 54 (1996) 12049.
[21] H. Liu, C. Jin, Y. Zhao, Physica B 315 (2002) 210.
[22] M.I. McMahon, C. Hejny, J.S. Loveday, L.F. Lundegaard, M. Hanfland, Phys. Rev. B 70 (2004) 054101.
[23] T.A. Grandi, V.H. dos Santos, J.C. de Lima, Solid State Commun. 112 (1999) 359.
[24] G. Lucazeau, J. Raman Spectrosc. 34 (2003) 478.